JOURNAL OF VIROLOGY, Oct. 1997, p. 7448–7460 Vol. 71, No. 10
0022-538X/97/$04.00+0

Baculovirus *gp64* Gene Expression: Negative Regulation by a Minicistron

MIN-JU CHANG AND GARY W. BLISSARD*

Boyce Thompson Institute at Cornell University, Ithaca, New York 14853

Received 10 April 1997/Accepted 18 July 1997

Small upstream open reading frames (ORFs) or minicistrons located in the 5′ leader of eukaryotic mRNAs have been shown to play a role in translational regulation of some eukaryotic genes, particularly mammalian proto-oncogenes. A survey of the baculovirus *Autographa californica* multicapsid nuclear polyhedrosis virus genome suggests that at least 10 transcripts from late genes contain potential minicistrons, and at least three of these minicistrons appear to be conserved in homologous genes of the related *Orygia pseudotsugata M*NPV. The position of the minicistron from one of these genes, *gp64*, is also conserved in *gp64* genes from several baculoviruses, suggesting a potential regulatory function. To identify the potential role of the *gp64* minicistron in regulating translation from *gp64* late mRNAs, we generated a series of recombinant viruses containing the *gp64* promoter and minicistron in combination with a chloramphenicol acetyltransferase reporter gene (*cat*) inserted into the polyhedrin locus. We first fused a *cat* reporter in frame with the minicistron coding region to demonstrate that the minicistron initiator ATG was in a context suitable for translational initiation. In subsequent experiments, a *cat* reporter was fused in frame to the downstream *gp64* ORF, and various constructs containing point mutations that inactivated the minicistron were examined. Translational efficiency in the presence and absence of the minicistron was measured by quantitative analysis of *gp64-cat* RNA and the GP64-CAT protein. In the absence of a functional minicistron, translational efficiency from the downstream *gp64-cat* reporter ORF increased. Surprisingly, single-point mutations that inactivated the minicistron initiator ATG also resulted in utilization of an upstream in-frame ATG that is found within the minicistron coding region and that is in a poor translational initiation context. Double-point mutation constructs that inactivated both the minicistron initiator ATG and the upstream in-frame ATG also resulted in increased translational efficiency from the downstream *gp64-cat* ORF. Thus, the *gp64* minicistron serves as a negative regulatory element that decreases translation of the *gp64* ORF on late mRNAs.

Baculoviruses are large double-stranded DNA viruses with genomes of 80 to 180 kbp. Three of the most widely studied baculoviruses, *Autographa californica* multicapsid nuclear polyhedrosis virus (Ac*M*NPV), *Bombyx mori* NPV (BmNPV), and *Orgyia pseudotsugata M*NPV (Op*M*NPV), have been completely sequenced and have genomes of approximately 134, 128, and 132 kbp, respectively (1, 4, 46). Baculoviruses in the NPV group replicate and are transcribed in the nuclei of infected cells. The infection cycle consists of early, late, and very late phases, and regulation of these phases appears to be determined primarily at the level of transcription (26). Early genes are transcribed by host RNA polymerase II prior to viral DNA replication (20, 24, 72). Late genes are transcribed by a virus-induced RNA polymerase activity that appears to be encoded mostly by viral genes (5, 20, 33, 45, 49, 67). The late RNA polymerase activity recognizes late and very late baculovirus promoters which consist of the almost invariant core TAAG sequence and a limited amount of flanking sequence (21, 51, 58, 60). Like host mRNAs, baculovirus transcripts are capped (68). However, viral RNA splicing appears to be extremely rare, since only a single spliced gene has been identified (14).

Early and late viral mRNAs are translated in the cytoplasm, and translation is thought to be mediated by host ribosomes and cofactors. Little is known regarding viral regulation or control of translation. However, several studies suggest that the regulation of translation plays an important role in viral infection, since an apparent translational inhibition has been associated with viral host range restriction (27, 35). Consensus translational initiation contexts derived from mammalian systems appear to be functional in recombinant baculoviruses; however, highly expressed baculovirus genes such as polyhedrin and p10 do not necessarily conform to optimal translational initiation sequences established in mammalian systems (60). In several instances, transcriptional mapping studies have identified sets of overlapping baculovirus mRNAs that are coterminal at either the 5′ or the 3′ end (7, 8, 19, 22, 23, 53, 66). These overlapping mRNAs may contain as many as five major open reading frames (ORFs) and thus are structurally multicistronic. Transient expression studies of multicistronic mRNAs from Op*M*NPV showed that these multicistronic mRNAs were translated primarily as monocistronic mRNAs (23). These data suggest that in baculovirus-infected cells, ribosomes enter and scan viral mRNAs from the capped 5′ end, as observed from mRNAs in eukaryotic cells.

mRNAs transcribed from some baculovirus genes contain very small ORFs (minicistrons) within the upstream leader region. Potential minicistrons have been reported in the *gp64* (8), *pp31* (25), *p143* (44), and *gp37* (71) genes of the Op*M*NPV and Ac*M*NPV baculoviruses. It is not known if these minicistrons are translated or whether the short peptides encoded by the minicistrons have a function. However, in each case the major downstream ORF is translated from the mRNA containing the minicistron. In mammalian systems, upstream AUG codons on mRNAs of proto-oncogenes are frequently observed (40), and some have been shown to encode minicis-

* Corresponding author. Mailing address: Boyce Thompson Institute, Cornell University, Tower Rd., Ithaca, NY 14853-1801. Phone: (607) 254-1366. Fax: (607) 254-1366. E-mail: gwb1@cornell.edu.

trons that play a role in the regulation of translation of the downstream ORF (3, 28, 47).

In the present study, we analyzed the Ac*M*NPV genome and found that at least 10 late genes contain potential upstream minicistrons. Of the *gp64* genes examined from three distinct baculoviruses (Op*M*NPV [8], Ac*M*NPV [70], and *Choristoneura fumiferana M*NPV [29]), all appear to have minicistrons in a conserved regulatory context. The transcription of *gp64* genes from Op*M*NPV and Ac*M*NPV has been studied in some detail (8, 9, 21, 34, 37). In these viruses, early transcripts initiate within −43 and −38 nucleotides (nt), respectively, upstream of the *gp64* ORF, and late transcripts initiate farther upstream. In *gp64* genes from both viruses, a minicistron is found on late but not early transcripts. Although these minicistrons differ in size and coding sequence, their locations relative to early and late transcription start sites are conserved. Analyses of sequences from additional *gp64* genes from BmNPV (46), *Anticarsia gemmatalis M*NPV (53a), and *Rachiplusia ou M*NPV (2) indicate that the same late promoter-minicistron-early promoter structure is present in those viruses. Because this promoter-minicistron structure is conserved in several distinct baculoviruses, we examined the function of the *gp64* minicistron in regulating the translational efficiency of the downstream ORF.

In addition to the AUG codon that initiates the five-amino-acid minicistron, a second upstream AUG codon is found within the 5′ leader of Ac*M*NPV *gp64* late transcripts. This second AUG is in frame with the downstream *gp64* ORF (70) but is in a poor translational initiation context as defined in mammalian cells. Because this second upstream in-frame AUG is in frame with the downstream *gp64* ORF, it was originally identified as a potential start codon of the *gp64* ORF (70). However, based on transcriptional mapping data (21, 34), homologies with Op*M*NPV GP64 (which contains no upstream in-frame AUG) (8), and the signal peptide predicted from N-terminal peptide analysis of the mature protein (64), it is clear that the third AUG serves as the authentic *gp64* initiation codon.

In the present study, we examined the role of the upstream *gp64* minicistron in translational efficiency of the Ac*M*NPV *gp64* ORF during the late phase of infection. To accomplish this, we constructed recombinant Ac*M*NPVs that contained the Ac*M*NPV *gp64* promoter region and a *gp64-cat* reporter fusion in the polyhedrin locus. To examine the effects of the minicistron and upstream AUGs, these potential upstream initiation codons were removed by introducing nucleotide substitution mutations. The effects of the absence of the minicistron and second upstream AUG were monitored by both CAT assays and quantitative immunoprecipitation of the CAT reporter protein.

MATERIALS AND METHODS

Reporter gene construction. (i) Minicistron-*cat* fusion. A *cat* ORF was fused in frame with the *gp64* minicistron, and the construct was inserted into a recombinant baculovirus. A truncated *gp64* promoter sequence was PCR amplified from plasmid pBS-Ac Sal/Bgl, which contains the full-length Ac*M*NPV *gp64* gene. Two primers, AcP5′ (GB134 [5′-ACAGCCAGATAAAACCCGGGTTAT CAAT-3′]) and MiniBamAc (GB172 [5′-CGGGATCCATTGAGGCATCTTA TAT-3′]), were used to create an *Ava*I (*Sma*I) site at the 5′ end and a *Bam*HI site at the 3′ end of an amplified *gp64* promoter which contained sequence from 147 bp upstream of the *gp64* ORF through the fourth codon of the *gp64* minicistron (−147 to −51 relative to the *gp64* ORF). The resulting *Ava*I-*Bam*HI fragment containing the late promoter and truncated minicistron was subcloned into the pBS-BglII plasmid vector to create a plasmid which was designated pAcMCt. A 1,019-bp *Bam*HI fragment containing a *cat* ORF with 36 bp of linker sequence at the 5′ end and 210 bp of 3′ untranslated sequence (from the 3′ end of the Op*M*NPV *gp64* gene) was excised from plasmid pTATA CAT (37) and subcloned into the *Bam*HI site of pAcMCt to create a minicistron-*cat* fusion construct, pAcMC-C. The resulting plasmid contained the *gp64* late promoter region and four codons of the *gp64* minicistron fused in frame to a linker and the *cat* ORF. Because all manipulations of sequences were at the DNA level, we will refer to the initiator codon as ATG (rather than AUG). To prevent translation initiation from the endogenous *cat* translational start site ATG (at +48 bp relative to the minicistron ATG), the endogenous *cat* initiator ATG was eliminated by site-directed mutagenesis. Primer ATGCAT-del (GB174 [5′-CCAGTG ATTTTTTTCTCAGATCTAGCTTCCTTAGC-3′]) was used with a *Dpn*I-based site-directed mutagenesis kit (5prime3prime, Inc.) to create a *Bgl*II site at the *cat* ATG sequence of pAcMC-C. The resulting plasmid was designated pAcMC-CAT. The promoter-minicistron-*cat* fusion construct was subcloned from pAcMCCAT as a 1,114-bp *Sma*I-*Xba*I fragment and was inserted between the *Eco*RV and *Xba*I sites of the pAcDZ1 transfer vector (74).

(ii) Inactivation of the *gp64* minicistron. A DNA fragment containing 147 bp upstream of the Ac*M*NPV *gp64* ORF plus 21 bp of the *gp64* ORF was amplified by PCR and cloned. Two primers, AcP5 (GB134) and AcP3 (GB135 [5′-GGG ATCCAAAACAATAGCGCTTAC-3′]), were used to introduce a *Sma*I (*Ava*I) site into the 5′ end and a *Bam*HI site into the 3′ end of the amplified fragment. This region was subsequently cloned into the *Ava*I-*Bam*HI sites of a pBS-BglII plasmid, and the resulting plasmid was designated pAcMC^{ATG}. To examine the effect of eliminating the *gp64* minicistron on translation from the downstream *gp64* ORF, two sets of minicistron mutations were generated. Point mutations were introduced into the minicistron by the long-primer unique-site-elimination mutagenesis technique (59). Primer AcP-ARG (GB137 [5′-GGTCGGGTATAT AAGARGCCTCAATGC-3′]) was used to change the initiator codon of the minicistron from ATG to either AaG or AgG. Primer USE-Eco (5′-ATACGA CTCACTATAGGGCGtATT C-3′) was used to eliminate the *Eco*RI site and as the other member of the primer pair. Plasmid pAcMC^{ATG} was used as the template. The resulting plasmids containing the above point mutations were designated pAcMC^{AaG} and pAcMC^{AgG}, respectively. To remove the methionine codon from within the minicistrons (or mutant minicistrons) of the above constructs (pAcMC^{ATG}, pAcMC^{AaG}, and pAcMC^{AgG}), primers ATGugTG (GB239 [5′-CTAGTAGCAcTGAGGCATC-3′]), AaGugTG (GB243 [5′-CTAGTAGCA cTGAGGCTTC-3′]), and AgGugTG (GB241 [5′-CTAGTAGCAcTGAGGCC TC-3′]) were used to change the internal minicistron ATG codon to gTG. The resulting plasmids were designated pAcMC$^{ATG\text{-}gTG}$, pAcMC$^{AaG\text{-}gTG}$, and pAcMC$^{AgG\text{-}gTG}$, respectively. A 1,019-bp *Bam*HI fragment containing the *cat* reporter gene cassette (described above) was subcloned into the *Bam*HI site of each promoter-minicistron construct (pAcMC$^{ATG\text{-}gTG}$, pAcMC$^{AaG\text{-}gTG}$, and pAcMC$^{AgG\text{-}gTG}$). The resulting promoter-reporter constructs contained a wild-type late *gp64* promoter, a wild-type or mutant minicistron, and a downstream *gp64-cat* reporter fusion. The *gp64-cat* reporter fusion consisted of 21 nt (seven amino acids) of the wild-type *gp64* ORF, 36 nt of linker sequence, and 660 nt of the *cat* ORF. The promoter-minicistron-reporter constructs were cloned into the pAcDZ1 transfer vector, as described above, to produce the following six constructs: pAcMC^{ATG}CAT, pAcMC^{AaG}CAT, pAcMC^{AgG}CAT, pAcMC$^{ATG\text{-}gTG}$CAT, pAcMC$^{AaG\text{-}gTG}$CAT, and pAcMC$^{AgG\text{-}gTG}$CAT. Each transfer vector construct was confirmed by nucleotide sequencing with primer Polh.2 (GB175 [5′-GTAATGAGACGCACAAAC-3′]), which binds upstream of the polyhedrin locus.

Recombinant virus production. BacPak 6 Viral DNA (Clontech Inc.) was purified by standard procedures (55) and was linearized by digestion with *Bsu*36I. Recombinant viruses were generated by cotransfecting linear BacPak 6 viral DNA and supercoiled plasmid transfer vector DNA into *Spodoptera frugiperda* Sf21 cells as previously described (36, 55). In all viral constructs, the polyhedrin promoter and ORF were removed and replaced by the *gp64* reporter constructs (see Fig. 1d). The wild-type *gp64* locus of each virus was unchanged. Recombinant viruses were purified by two rounds of plaque purification (55). Budded virus stocks were prepared at 4 days postinfection (p.i.) from Sf9 cells infected at a multiplicity of infection (MOI) of 0.1. To confirm normal regulation of gene expression in each recombinant virus, the temporal cascade of protein synthesis was analyzed by pulse-labeling proteins in infected cells at various times p.i. as described previously (43).

Analysis of CAT activity. Preparation of cell extracts and two-phase fluor diffusion CAT assays were performed essentially as described previously (6, 52). In 24-well plates (15.5-mm-diameter wells), 3×10^5 Sf9 cells were plated in each well and infected with recombinant viruses at an MOI of 20. At 24 h p.i., the cells were washed twice with phosphate-buffered saline (PBS) and resuspended in 100 μl of PBS plus 5 mM EDTA. The cells were lysed by three cycles of freezing at −70°C and thawing at 37°C for 1 min. After pelleting cell debris, cell lysates were stored at −20°C. For CAT assays, extracts were diluted 1:20 in PBS, and a volume of 120 μl of the diluted cell extract was used in a total CAT assay reaction volume of 250 μl, containing 7 or 10 μCi of [^{3}H]acetyl coenzyme A (1 Ci/mmol [New England Nuclear]) and 1 mM chloramphenicol (Sigma) as substrates. For each recombinant virus, five replicate wells of cells were infected and analyzed by CAT assays. All data analyzed from each sample fell within the linear range of the CAT assay. Extracts from uninfected Sf9 cells (mock) and wild-type Ac*M* NPV-infected Sf9 cells were used for calculations of background in CAT assays. CAT standards (Sigma) were included in each experiment as positive controls.

Quantitative immunoprecipitation of CAT protein. Sf9 cells were plated in 24-well plates and infected with recombinant viruses as described above for CAT assays. Metabolic labeling and quantitative immunoprecipitation of CAT protein were performed as previously described (54), with modifications. Infected Sf9

TABLE 1. Minicistrons present in transcriptionally mapped late genes of Ac*M*NPV[a]

ORF no.	Gene name	Leader length (nt)	MC position (bp)	MC initiator context	MC size (amino acids)	IC distance (nt)
7	*orf 7*	105[b]	4,409 < 4,432	TCC **ATG** A	7	44
31	*sod*	216,[b] 11	25,757 > 25,807	GGC **ATG** T	16	12
36	*pp31/39k*	158[b]	30,172 < 30,186	CAA **ATG** T	4	102
64	*gp37(34.8k)*	90,[b] 14	52,213 < 52,269	ATT **ATG** T	18	21
89	*vp39*	382,[b,c] 107, 59	76,763 < 76,783	ATT **ATG** T	6	185
95	*helicase/p143*	166,[b] 73[b]	84,410 < 84,427	AGA **ATG** G	5	50
104	*vp80*	36[b]	89,537 > 89,554	CAC **ATG** G	5	9
105	*he65*	93[b]	93,374 < 93,418	TAT **ATG** C	14	45
128	*gp64/gp67*	139,[b] 126[b]	109,762 > 109,779	AAG **ATG** C	5	44
138	*p74*	90[b]	121,119 < 121,142	TAA **ATG** T	7	46

[a] The designated numbers of the major ORFs, gene names, and locations and orientations of the minicistrons in the Ac*M*NPV genome (MC position) follow the previously established nomenclature (4). The lengths of 5′ leader sequences are listed (leader length), and the immediate context of the ATG codon that initiates the minicistron (MC initiator context) and the length of each minicistron in codons (MC size) are indicated. Intracistronic distance (IC distance) indicates the distance between the termination codon of the minicistron and the ATG initiator of the major downstream ORFs listed on the left.

[b] Leader-containing minicistron.

[c] The minicistron identified from the *vp39* gene is found on a very long transcript that represents only a small fraction of the *vp39* mRNAs expressed in the late phase (66).

cells were incubated for 30 min in methionine-free Grace's medium prior to labeling. A total of 72.5 μCi of Express Protein Labeling mix ([^{35}S]methionine/cysteine; 1,175 Ci/mmol; Dupont NEN) in 250 μl of methionine-free Grace's medium was added to each well of the 24-well plate, and the plate was incubated for 30 min. After labeling, the cells were placed at 4°C and processed as follows. The cells were lysed in 300 μl of RIPA buffer (150 mM NaCl, 50 mM Tris, 1% Nonidet P-40, 0.5% deoxycholate, 0.1% sodium dodecyl sulfate [SDS]) containing a protease inhibitor cocktail (0.5-μg/ml leupeptin, 0.7-μg/ml pepstatin, 1-mg/ml Pefabloc SC hydrochloride; Boehringer Mannheim) for 45 min. From each cell lysate, 50 μl (5×10^4 cell equivalents) was removed and mixed with 2 μl of anti-CAT antiserum (5prime3prime, Inc.), and the mixture was incubated for 30 min at 4°C. A volume of 15 μl of Staph-A suspension (1:10 [wt/vol]; Pearce) was added to the lysate-antiserum mixture, and the mixture was incubated for another 30 min at 4°C. After three washes by pelleting and resuspension in 300 μl of RIPA buffer, immunoprecipitates were pelleted and resuspended in Laemmli sample buffer. Each sample was denatured by incubation at 100°C for at least 10 min and then electrophoresed on SDS-12% polyacrylamide gel electrophoresis (PAGE) gels. The gels were vacuum dried and exposed on PhosphorImager screens for 12 h and then scanned on a Molecular Dynamics PhosphorImager (model 400A). To ensure that antibodies were in excess in quantitative immunoprecipitation experiments, titration experiments were conducted (see Fig. 4a). Using the same procedure and extracts, a parallel immunoprecipitation experiment was conducted with an anti-GP64 monoclonal antibody, AcV1 (32).

RNA isolation and primer extension analysis. For isolation of viral RNA, Sf9 cells (1.5×10^7) were plated in 150-cm^2 T flasks and infected with each recombinant virus at an MOI of 20, and the flasks were then incubated at 27°C for 24 h. Total RNA was isolated as described previously (7). Primer extension reactions were performed as described previously (6), with the following modifications. Two primers, Pr64wt (GB169 [5′-GCTCCGCCGCAAAGGCAGAATGCC-3′]) and PrCAT1 (GBBT80 [5′-TTCTTTACGATGCCATTGGG-3′]), which were complementary to the 5′ end of the Ac*M*NPV *gp64* ORF or the *cat* reporter ORF, respectively, were used for primer extension reactions. Approximately 20 pmol of each oligonucleotide primer was 5′ end labeled with ^{32}P in a 50-μl reaction mixture containing 10 U of T4 polynucleotide kinase, 120 μCi of [^{32}P]ATP (6 Ci/mmol), and 1× kinase buffer (50 mM Tris [pH 7.5], 10 mM $MgCl_2$, 5 mM dithiothreitol, 0.5 mM spermidine). After incubation at 37°C for 1 h, reactions were terminated by the addition of 1 μl of 0.5 M EDTA and incubation at 65°C for 15 min. Labeled primers were precipitated in 0.2 M $MgCl_2$–2 volumes of ethanol–20 μg of glycogen. The specific activity of each labeled primer was adjusted to 10^6 cpm/pmol by adding unlabeled primer and water. Quantitative primer extension reactions were performed in a total volume of 40 μl containing 3 μg of total RNA annealed with 4 pmol of labeled primers (10^6 cpm/pmol) in 50 mM Tris (pH 8.0)–50 mM KCl–5 mM $MgCl_2$–50 mM dithiothreitol–0.25 mM each deoxynucleoside triphosphate. Each reaction mixture contained 5 U of avian myeloblastosis virus Reverse Transcriptase (Promega) and was incubated at 50°C for 45 min. To avoid evaporation, 50 μl of mineral oil was layered above each primer extension reaction mixture. Reactions were terminated by the addition of 1 μl of 0.5 M EDTA, and a 5′-end-labeled 164-bp DNA fragment was added to each sample as a precipitation and loading control. RNAs were then eliminated by the addition of 1 μg of RNase and incubation for 20 min at 37°C. Chloroform extraction was performed on each reaction to remove mineral oil, and the primer extension products were precipitated with 3 volumes of ethanol and 1 volume of 2.5 M NH_4OAc. Primer extension products were resuspended in 5 μl of stop solution (95% formamide, 20 mM EDTA, 0.05% bromophenol blue, 0.05% xylene cyanol FF) and analyzed on 6% polyacrylamide–7 M urea sequencing gels. The sizes of labeled primer extension products were determined by comparisons to DNA-sequencing ladders generated by dideoxy sequencing of the pBS-BglII plasmid with reverse primers. The gels were dried, exposed on PhosphorImager screens, and imaged on a PhosphorImager, and the primer extension products were quantified with ImageQuant software (Molecular Dynamics). To make quantitative measurements of transcripts, preliminary primer extension experiments were performed to ensure that labeled primers were in excess in primer extension reactions (see Fig. 4a). Various quantities of RNA (1 to 10 μg) were annealed to 4 pmol of primers (10^6 cpm/pmol) and were extended at 50°C for 45 min. Based on titration results, a quantity of 3 μg of total RNA from each sample was selected for use in the quantitative primer extension reactions. For each total RNA sample, primer extension experiments with each primer were repeated three times.

RESULTS

To determine the frequency of potential minicistrons in the Ac*M*NPV genome, we analyzed the published Ac*M*NPV genome sequence (4) to identify possible minicistrons upstream of each of the 154 potential major ORFs. The criteria used for this search were the following. (i) Searches were limited to 200 bp upstream of each major ORF or to the length of the longest transcript for transcriptionally mapped genes. (ii) All ATGs present within the designated upstream region were examined. (iii) Small ORFs with a coding capacity of 2 to 30 amino acids were selected for analysis. We identified 104 genes that may contain minicistrons. Since only approximately 36 genes in the Ac*M*NPV genome have been transcriptionally mapped, we do not know if all minicistrons identified using these criteria are present in baculovirus transcripts. To extend our analysis, we searched for potential late promoters upstream of the 104 genes containing potential minicistrons. The core late promoter sequence 5′-G/T/A TAAG-3′ was used as an indicator of potential late promoters. From the 104 genes selected above, we identified 27 genes that contain minicistrons within potential late transcripts. Of these, 10 genes (*orf7*, *sod*, *pp31/39k*, *gp37*, *vp39*, *helicase*, *vp80*, *he65*, *gp64/gp67*, and *p74*) have been mapped transcriptionally and are thus confirmed as containing minicistrons on late transcripts. The relative positions, sizes, and translational contexts of these minicistrons are indicated in Table 1. Interestingly, only the minicistron from the *helicase* gene contains an optimal translational start site context, as defined for mammalian cells (42). This relatively high frequency of minicistrons in Ac*M*NPV late transcripts (10 minicistrons identified in the 5′ leaders of approximately 36 mapped transcripts) suggests that minicistrons may serve as a

general regulatory mechanism which is present in a number of late genes.

Transcription of the *gp64* gene in Ac*M*NPV and Op*M*NPV has been studied in detail (6, 8, 9, 21, 34, 37, 38). In the Ac*M*NPV *gp64* promoter region, the early transcription start site is located downstream of two late transcription start sites (Fig. 1a). A minicistron that encodes a small peptide (MPQCY) is located on late transcripts, but not on early transcripts. To examine the functional significance of the Ac*M*NPV *gp64* minicistron, we used two strategies. First, a reporter gene was fused to the *gp64* minicistron (Fig. 1b) to determine whether translation initiates from the minicistron ATG on late transcripts. Then, we examined the effect of the minicistron on translation of the *gp64* ORF. To accomplish this, a reporter gene was fused in frame to the *gp64* ORF and point mutations were used to inactivate the minicistron (Fig. 1c). For all experiments, we constructed recombinant Ac*M*NPVs containing the appropriate late promoter-minicistron constructs in the polyhedrin locus (Fig. 1d).

Translation from the minicistron ATG. To determine whether the putative ATG initiation codon of the minicistron was competent to initiate translation on late mRNAs, we generated a construct containing promoter-minicistron sequences from −147 to −51 (relative to the *gp64* translation start site at +1) and a *cat* ORF fused in frame with the minicistron (Fig. 2a). The resulting construct contained 12 nt from the *gp64* minicistron (4 codons) fused in frame to a 36-nt linker region (12 codons) and the *cat* ORF (in which the *cat* initiator ATG was inactivated) under the control of *gp64* late promoters (Fig. 2a). A recombinant virus, vAcMCCAT, containing this construct was generated and analyzed.

We detected substantial levels of CAT activity from lysates of vAcMCCAT-infected Sf9 cells during the late phase (24 h p.i.), and only minimum levels of CAT activity from extracts of BacPak 6- or mock-infected cells which served as negative controls (Fig. 2b). As a positive control, CAT activity was also measured from Sf9 cells infected with virus vAcMC^{ATG}, which contained a *gp64-cat* fusion (Fig. 1c, vAcMC^{ATG}) under the control of the wild-type *gp64* promoter. The substantial CAT activity detected from vAcMCCAT indicated that the minicistron ATG was sufficient to initiate translation from Ac*M*NPV late mRNAs.

To confirm that the CAT activity detected in the previous experiment resulted from initiation at the minicistron ATG, we immunoprecipitated the CAT fusion protein from cells infected with vAcMCCAT and compared the fusion protein with the wild-type CAT protein (Fig. 2c). Lanes 1 and 2 show negative controls from cell lysates of either mock- or BacPak 6-infected cells. Lane 3 shows CAT protein immunoprecipitated from cells infected with a recombinant virus, vAcP(21/20)min, that expressed an unfused, wild-type CAT protein (21). The predicted translation product from the minicistron-CAT fusion protein from vAcMCCAT was approximately 2 kDa larger than the native CAT protein. The measured size of the immunoprecipitated CAT fusion protein was consistent with the prediction (Fig. 2c, lane 3 versus lane 4). Thus, CAT activity and immunoprecipitation data from these recombinant viruses indicate that the *gp64* minicistron ATG is found in a context that is utilized in the late phase of infection.

Inactivation of the minicistron ATG initiator codon. The conservation of the *gp64* minicistron in several baculoviruses suggests an important role for this structure. To understand the role of the minicistron and to measure its effect on translation of the downstream *gp64* ORF, we generated a reporter construct in which a *cat* ORF was fused in frame to the downstream *gp64* ORF. We then inactivated translation of the up-

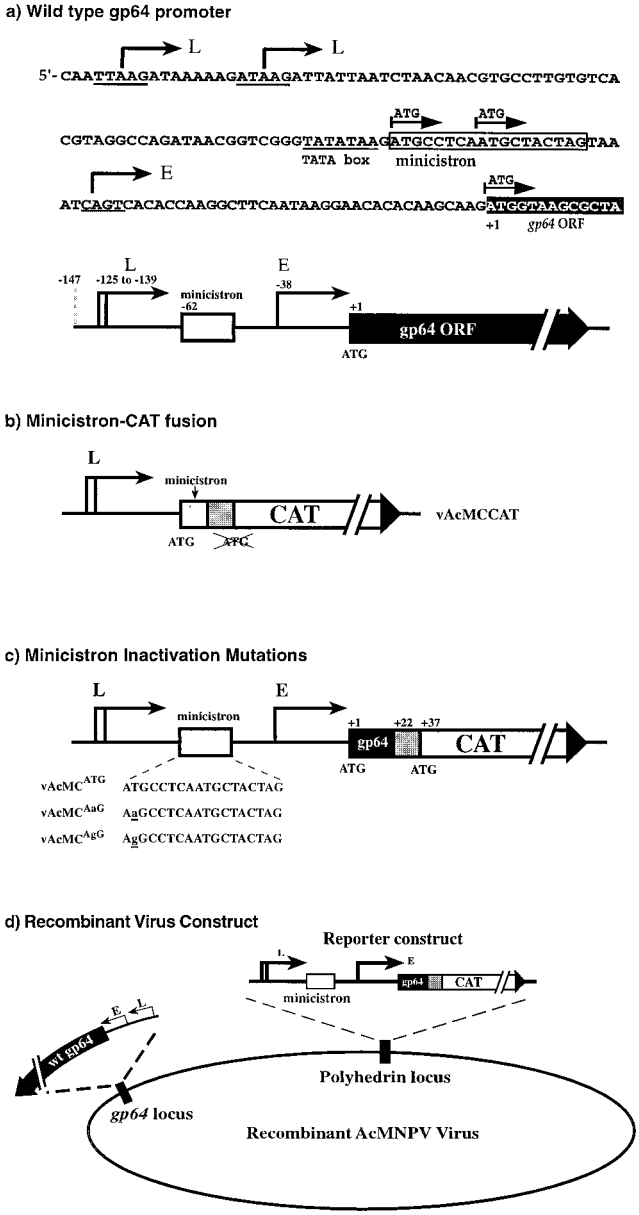

FIG. 1. Ac*M*NPV *gp64* promoter region, mutational strategy, and recombinant viruses. (a) The DNA sequence and a diagram of the wild-type Ac*M*NPV *gp64* promoter and upstream region show the relative positions of the early (E) and late (L) transcriptional start sites (21) and the location of the minicistron (open box) relative to the *gp64* translational start site (ATG at +1) and *gp64* ORF (black box). (b) *gp64* minicistron-*cat* reporter fusion construct (vAcMC-CAT). The first four codons of the minicistron were fused to a linker of 36 bp (gray box) and a *cat* ORF in which the *cat* ATG was eliminated by site-directed mutagenesis. (c) A minicistron inactivation mutation strategy is illustrated. A 36-bp linker and *cat* reporter ORF were fused in frame, after the seventh codon of the *gp64* ORF. The translational start site ATG of CAT in this construct was not modified. The *gp64-cat* reporter fusion, therefore, contains the wild-type *gp64* initiator ATG at +1 and a downstream in-frame *cat* ATG at nucleotide +37. To eliminate the minicistron, the translational start site ATG of the minicistron was changed to AaG or AgG, as indicated in the name of each mutant virus construct (vAcMC^{AaG} or vAcMC^{AgG}, respectively). Lowercase letters indicate the positions of substitution mutations. (d) The strategy used for constructing the recombinant viruses generated in this study. All reporter constructs were cloned into the polyhedrin locus of Ac*M*NPV, replacing the polyhedrin gene, while the *gp64* locus remained unchanged. wt, wild type.

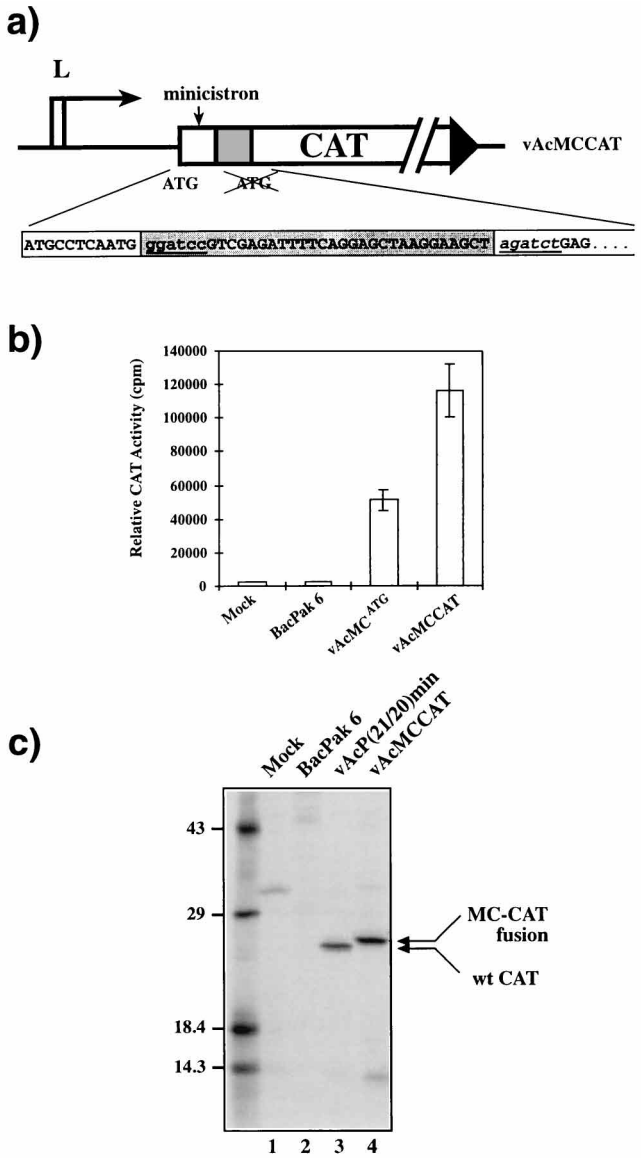

FIG. 2. CAT expression from a recombinant Ac*M*NPV containing a minicistron-*cat* fusion. (a) Structure and sequence of the minicistron-*cat* fusion inserted in the Ac*M*NPV polyhedrin locus. The structure of the vAcMCCAT construct is shown, with sequence from the minicistron, linker, and *cat* ORF given below. Virus vAcMCCAT contains the *gp64* late promoter and a portion of the minicistron fused to a *cat* cassette. Linker sequences connecting the *gp64* minicistron and *cat* ORF are shown in the gray box, and restriction sites are underlined. The nucleotide changes used to inactivate the bacterial *cat* ORF ATG are indicated by italics. (b) CAT activity from cells infected with vAcMCCAT and vAcMC^{ATG}. Sf9 cells were infected with recombinant viruses vAcMCCAT (which contains the minicistron-*cat* fusion) and vAcMC^{ATG} (which contains a wild-type minicistron and a *cat* reporter fused to the downstream *gp64* ORF) (Fig. 1) or BacPak 6 (a negative control virus). Mock, cells that were not infected with virus. Relative CAT activities from 24 h p.i. extracts were measured by a two-phase fluor diffusion assay (52) and are given as counts per minute. (c) Immunoprecipitation of fused and unfused CAT proteins. CAT proteins from Sf9 cells mock infected or infected with recombinant viruses BacPak 6, vAcMCCAT, and vAcP(21/20)min (21) were metabolically labeled with [^{35}S]Met/Cys for 30 min at 24 h p.i. and then immunoprecipitated with anti-CAT antiserum and examined on SDS-PAGE gels. The sizes of marker proteins are indicated in kilodaltons on the left. wt, wild type.

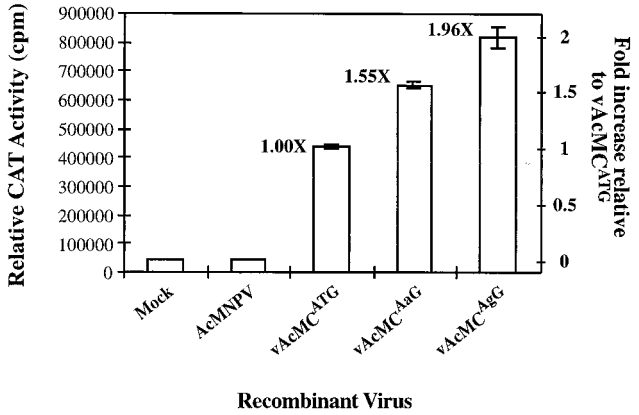

FIG. 3. Cumulative CAT activity from cells infected with recombinant virus constructs containing minicistron inactivation mutations. Sf9 cells were infected with wild-type or recombinant viruses at an MOI of 20, and cell extracts were generated at 24 h p.i. Average relative CAT activities from five replicates of each infection were determined by two-phase fluor diffusion assay and are presented as counts per minute (left). The CAT activities from cells infected with minicistron mutation viruses (vAcMC^{AaG} and vAcMC^{AgG}) were compared with those from cells infected with the wild-type minicistron virus (vAcMC^{ATG}). The fold increases above the wild-type virus construct are indicated beside each bar, and the scale is shown on the right.

stream minicistron and examined qualitative and quantitative effects on translation of the downstream ORF (Fig. 1c). To inactivate the minicistron, the minicistron translational start site ATG was substituted with either AaG or AgG in the reporter constructs. Several recombinant viruses were initially generated, and these included vAcMC^{ATG}, which contained a wild-type minicistron and initiator ATG codon; vAcMC^{AaG}, which contained an AaG substitution at the minicistron initiator position; and vAcMC^{AgG}, which contained an AgG substitution at the minicistron initiator position (Fig. 1c). These mutations inactivate the minicistron initiator codon while preserving the structure surrounding the adjacent TATA box, which is located immediately upstream of the minicistron ATG initiator (Fig. 1a). In these constructs, a CAT cassette was fused to the seventh codon of the *gp64* ORF. Thus, initiation downstream of the minicistron will occur at the authentic *gp64* ATG initiator. Because GP64 coding sequences included in these constructs did not include the intact signal peptide, this GP64-CAT fusion was not secreted (data not shown). These reporter constructs were analyzed by CAT assays and by quantitative immunoprecipitation of the GP64-CAT fusion protein, as described above.

(i) Cumulative CAT assay. Previous studies have shown that the *gp64* gene is expressed under the control of both early and late promoters. The minicistron is found only on late mRNAs that appear to be responsible for the majority of GP64 synthesis (8, 21, 34, 50). Although CAT activity detected from the recombinant virus-infected cells at 24 h p.i. represents CAT expressed during both early and late phases, late mRNAs predominate at that time. Only CAT translated from late mRNAs (containing the minicistron) should be affected by the presence or absence of the minicistron. To aid in the interpretation of CAT assay data, we first performed an enzyme-linked immunosorbent assay (ELISA) to measure relative levels of GP64 from extracts of Ac*M*NPV-infected cells at various times p.i. In that experiment (data not shown), we determined that $\geq$78% of the GP64 protein detected at 24 h p.i. appears to be expressed during the late phase and is, therefore, subject to possible translational regulation by the minicistron. This is consistent with the observation that by 24 h p.i., late mRNAs constitute the majority of *gp64* mRNAs (21, 34). Figure 3 shows the result of CAT assays from cells infected with the recombinant viruses that carry a wild-type minicistron con-

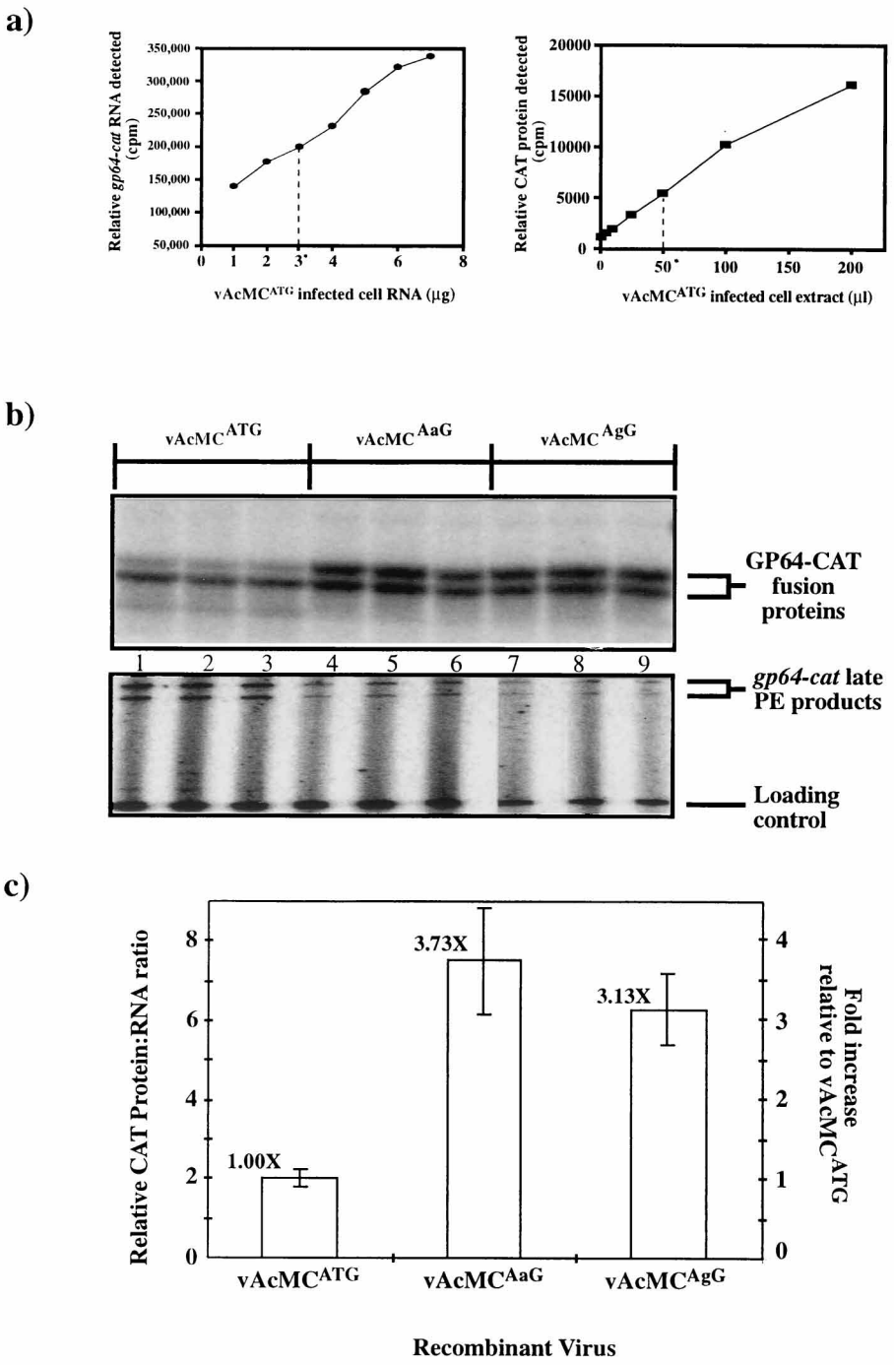

FIG. 4. Analysis of minicistron inactivation mutations by quantitative immunoprecipitation. Sf9 cells were infected with recombinant viruses at an MOI of 20. At 24 h p.i., cells were lysed, total RNA was isolated, and the CAT fusion proteins were immunoprecipitated with an anti-CAT antiserum. (a) Titrations of total RNA and CAT fusion protein for quantitative analysis. The left panel shows a quantitative analysis of late *cat* RNAs from a primer extension experiment in which 4 pmol of labeled PrCAT1 primer (complementary to the *cat* ORF) was used in primer extension reactions with increasing quantities (1 to 7 μg) of total RNA isolated from cells infected with virus vAcMC^{ATG}. A dashed line shows the quantity of RNA (3 μg) selected for use in subsequent quantitative primer extension experiments. The right panel shows a quantitative analysis of CAT proteins immunoprecipitated from increasing quantities (0 to 200 μl) of extracts from vAcMC^{ATG}-infected cells that were pulse-labeled with [^{35}S]Met/Cys for 30 min at 24 h p.i. Anti-CAT antiserum (2 μl) was used to immunoprecipitate the CAT protein. A dashed line indicates the quantity of extract (50 μl) selected for use in subsequent quantitative immunoprecipitation experiments. (b) Quantitative primer extension analysis of *gp64-cat* RNA and immunoprecipitation of GP64-CAT protein. Immunoprecipitation of GP64-CAT protein (upper panel) and primer extension of corresponding *gp64-cat* RNAs (lower panel) were performed with extracts from cells infected with recombinant viruses vAcMC^{ATG}, vAcMC^{AAG}, and vAcMC^{AGG}. PhosphorImager scans of three replicates of each quantitative immunoprecipitation and each quantitative primer extension reaction are shown. A labeled DNA fragment was added to each primer extension reaction prior to electrophoresis as an internal control (loading control). The positions of immunoprecipitated GP64-CAT proteins and primer extension products are indicated on the right. Labeled proteins and RNAs were quantified by PhosphorImager analysis. (c) Relative CAT protein-to-RNA ratios (indicated on the left axis) were calculated from data derived from an analysis of the gels shown in panel b. Fold increases relative to data from the vAcMC^{ATG} construct are indicated on the right and above each bar.

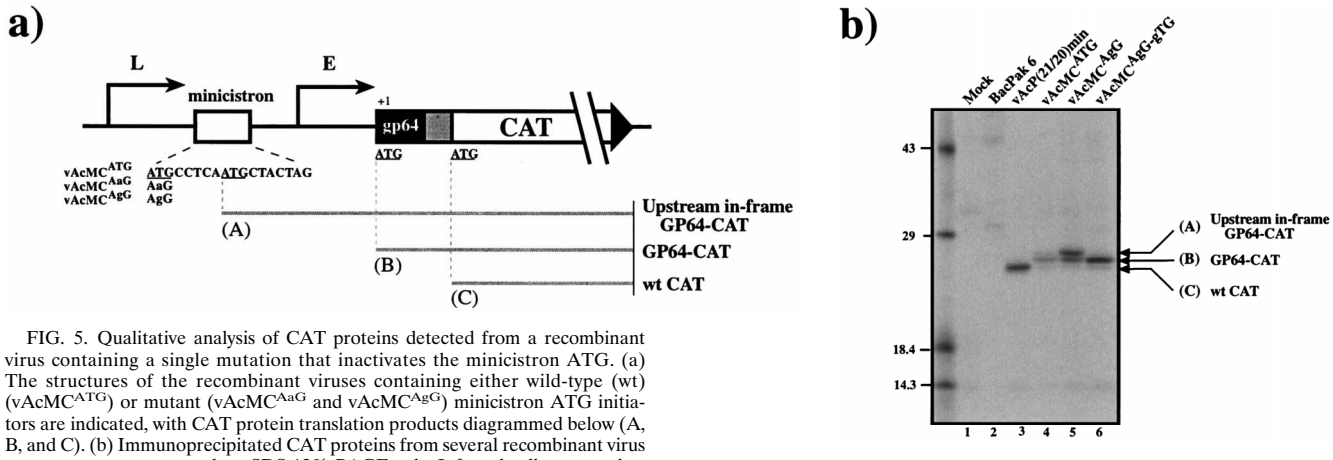

FIG. 5. Qualitative analysis of CAT proteins detected from a recombinant virus containing a single mutation that inactivates the minicistron ATG. (a) The structures of the recombinant viruses containing either wild-type (wt) (vAcMC^{ATG}) or mutant (vAcMC^{AaG} and vAcMC^{AgG}) minicistron ATG initiators are indicated, with CAT protein translation products diagrammed below (A, B, and C). (b) Immunoprecipitated CAT proteins from several recombinant virus constructs were compared on SDS-12% PAGE gels. Infected cells were pulse-labeled for 30 min at 24 h p.i., and CAT proteins were immunoprecipitated with an anti-CAT antiserum as described in Materials and Methods. The size of the wild-type CAT protein (wt CAT) expressed from a control virus [vAcP(21/20) min (21)] is compared to those of CAT proteins immunoprecipitated from recombinant viruses containing either a wild-type minicistron (vAcMC^{ATG}), a single mutation that inactivates the minicistron ATG (vAcMC^{AgG}), or a double mutation that inactivates the minicistron and the upstream in-frame ATG (vAcMC$^{AgG\text{-}gTG}$). The predicted products translated from the *gp64* ATG (GP64-CAT) and the upstream in-frame ATG (upstream in-frame GP64-CAT) are indicated on the right of the gel and correspond to products A and B shown in panel a.

struct (vAcMC^{ATG}) or inactivated minicistrons (vAcMC^{AaG} and vAcMC^{AgG}). CAT activities detected from the vAcMC^{AaG} and vAcMC^{AgG} viruses at 24 h p.i. were on average 1.55- and 1.96-fold, respectively, higher than that from the virus containing the wild-type minicistron construct (vAcMC^{ATG}). Inactivation of the minicistron resulted in increased translation of the downstream ORF. These data provided the first indication that the *gp64* minicistron negatively regulates translation from the downstream *gp64* ORF. Because this analysis of CAT activity contains a low level of possible background activity from translation of accumulated early transcripts (that do not contain the minicistron), we then performed a more precise quantitative analysis of expression from the downstream ORF.

(ii) Quantitative immunoprecipitation and measurements of translation efficiency. To confirm the above result and to precisely analyze the effects of the minicistron on translation from the downstream ORF, we pulse-labeled and quantitatively immunoprecipitated CAT proteins to measure the relative amounts of GP64-CAT fusion protein translated during a 30-min time period, during the late phase (see below). To evaluate the effect of the minicistron on translation efficiency, the ratio between GP64-CAT protein translated and the steady-state level of *gp64-cat* mRNA was determined for each virus during the same time period. This method eliminates any possible effect of transcriptional changes (that may result from the minicistron mutations) on the analysis of translation. We first measured the relative steady-state levels of *gp64-cat* RNA at 24 h p.i. from cells infected with each virus construct. Quantitative primer extension analysis was used to estimate the *gp64-cat* mRNA levels. The quantity of total RNA used in primer extension assays was titrated to ensure that the primer was in excess, and the result of an RNA titration is shown in Fig. 4a (left panel). Using these primer extension conditions, we measured the *gp64-cat* reporter RNAs at 24 h p.i. from cells infected with the recombinant viruses (Fig. 4b, lower panel). To develop a quantitative immunoprecipitation assay, we first established conditions in which anti-CAT antibodies were in excess. Figure 4a (right panel) shows a titration experiment in which increasing quantities of labeled CAT protein were titrated against a standard quantity (2 μl) of an anti-CAT antiserum. Based on these results, 50 μl from each cell extract was used for quantitative immunoprecipitation experiments. Unexpectedly, two major GP64-CAT bands were consistently immunoprecipitated from cells infected with viral constructs containing the minicistron initiator codon mutations (Fig. 4b, top panel, lanes 4 to 9). The origins of these two bands are examined below; however, we will first discuss the quantitative effects of minicistron inactivation on the efficiency of overall downstream translation.

To determine the effect of minicistron inactivation, we quantified and compared GP64-CAT from the wild-type construct (containing an intact minicistron) to the two forms of GP64-CAT precipitated from the minicistron inactivation constructs (Fig. 4b, top panel; vAcMC^{AaG} and vAcMC^{AgG}, two major bands). Quantitative immunoprecipitation data from PhosphorImager scans of GP64-CAT bands (Fig. 4b, upper panel) were normalized to the corresponding steady-state level of *gp64-cat* RNA (Fig. 4b, lower panel), and the results are indicated in the graph in Fig. 4c. These data show that inactivation of the minicistron by point mutations in the minicistron initiator ATG resulted in increases of approximately 3.7- and 3.1-fold in translation from downstream sites. These experiments further indicate that the minicistron negatively regulates translation of the downstream ORF.

(iii) Analysis of multiple CAT proteins. Because two major GP64-CAT products were detected upon inactivation of the minicistron in the above experiments, we measured the sizes of the two CAT products and compared these sizes with those predicted from potential ATG initiation sites. While the lower band corresponds to the CAT fusion initiated at the *gp64* translation start codon, the upper band is approximately 2 kDa greater in size (Fig. 4b, upper panel, lanes 4 to 9). A diagram of the position of each ATG located downstream of the minicistron ATG is shown in Fig. 5a. A potential ATG initiator codon is found within the minicistron and is in frame with the downstream *gp64* ORF (Fig. 5a [upstream in-frame GP64-CAT]). Translation from this upstream in-frame ATG would result in a protein containing an additional 18 amino acids at the N terminus, with a predicted increase in mass of approximately 2 kDa. To examine this further, we immunoprecipitated CAT proteins from cells infected with three recombinant viruses and compared the relative sizes of the CAT fusion proteins (Fig. 5b). A control (unfused) wild-type CAT protein was

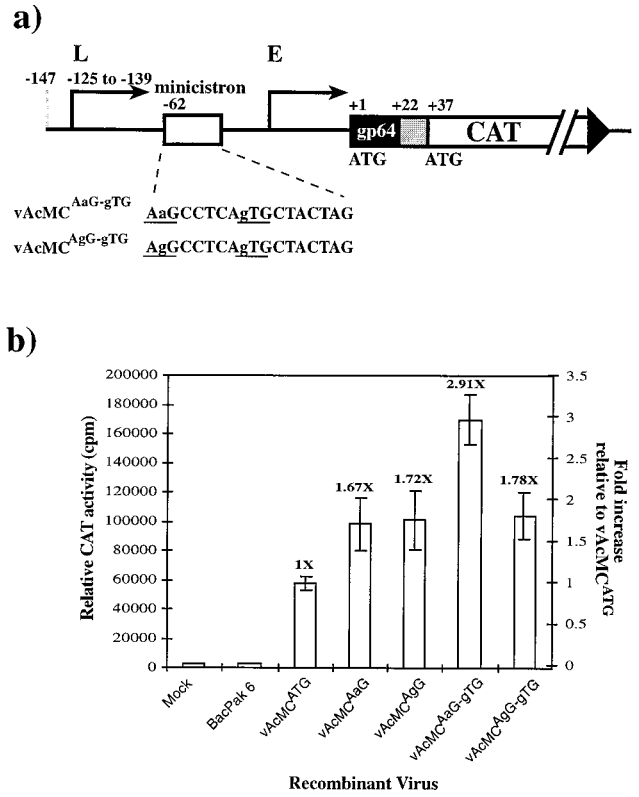

FIG. 6. Qualitative and quantitative analysis of CAT proteins detected from recombinant viruses containing double mutations that inactivate the minicistron ATG and the upstream in-frame ATG. (a) Structures of recombinant virus constructs containing mutant minicistron and upstream in-frame ATG initiators (vAcMC$^{AaG\text{-}gTG}$ and vAcMC$^{AgG\text{-}gTG}$). (b) Analysis of CAT activity from cells infected with recombinant viruses that contain either single or double mutations in the minicistron and upstream in-frame ATGs. Relative CAT activity is indicated on the left, and fold increases over activity from vAcMC^{ATG}-infected cells are indicated on the right and above each bar.

immunoprecipitated from cells infected with a virus containing a wild-type *cat* construct (Fig. 5b, lane 3 [21]). The major GP64-CAT fusion protein expressed in cells infected with the wild-type minicistron virus, vAcMC^{ATG}, was approximately 2 kDa larger than that from the unfused protein (Fig. 5b, lane 4 versus lane 3). In addition to the major band detected from the *gp64* initiator ATG (Fig. 5b, lane 4), two additional minor CAT bands were also detected (Fig. 5b, lane 4, and Fig. 4b, lanes 1 to 3). The lower CAT band corresponded to the size of the unfused wild-type CAT protein, while the upper band was approximately 2 kDa larger than GP64-CAT that initiated at the *gp64* ATG (Fig. 5b, lane 4). The size of the upper band corresponded to that predicted from a protein initiated at the upstream in-frame ATG, within the minicistron (Fig. 5a [A]). When the CAT protein was immunoprecipitated from cells infected with vAcMC^{AgG} (a viral construct containing an inactivated minicistron ATG [Fig. 5a]), we found that (i) two bands of approximately equal intensity were observed and (ii) the sizes of these bands were consistent with proteins translated from the upstream in-frame ATG and the *gp64* initiator ATG (Fig. 5a and b, lane 5). These data suggest that in the absence of a functional minicistron translational initiator (ATG), the ATG located within the minicistron ORF is used as a translational start site. Interestingly, this upstream in-frame ATG is not in a favorable context for translational initiation, as determined by Kozak for mammalian cells (42). Indeed, the approximately equal quantity of the smaller GP64-CAT protein (initiated downstream at the wild-type *gp64* ATG start site [Fig. 5b, lane 5]) indicates that translational initiation at the upstream site is leaky and suggests that the context at the upstream in-frame ATG site is not optimal for efficient translational initiation.

Inactivation of the minicistron and upstream in-frame initiator ATG codons. The above observations indicate that inactivation of the minicistron resulted in the utilization of an upstream in-frame ATG initiator codon that is not frequently utilized in the wild-type mRNA. To more accurately determine the quantitative effect of the minicistron on translation efficiency of the wild-type *gp64* ATG initiator, we inactivated both the minicistron ATG initiator codon and the upstream in-frame ATG codon found within the minicistron. In addition, inactivation of the upstream in-frame ATG codon would also confirm the origin of the larger GP64-CAT protein (Fig. 5b, lane 5). We predicted that in the absence of both the minicistron ATG (Fig. 5a [first ATG]) and the upstream in-frame ATG (Fig. 5a [A]), ribosomes would initiate translation at the (downstream) wild-type *gp64* ATG. We generated two additional virus constructs containing the same *gp64* promoter and upstream leader region, but with substitution mutations that inactivated both the minicistron ATG and the upstream in-frame ATG. The two additional recombinant virus constructs (Fig. 6a [vAcMC$^{AaG\text{-}gTG}$ and vAcMC$^{AgG\text{-}gTG}$]) were generated by an A-to-G point mutation in the upstream in-frame ATG codon of each of the transfer vectors used to generate vAcMC^{AaG} and vAcMC^{AgG}.

(i) Origin of the larger CAT fusion protein. To confirm the origin of the larger GP64-CAT protein (Fig. 5b, lane 5), we compared the sizes of CAT proteins immunoprecipitated from cells infected with vAcMC^{AgG} (which contains an inactivated minicistron initiator ATG) and vAcMC$^{AgG\text{-}gTG}$ (virus that contains an inactivated minicistron initiator ATG and an inactivated upstream in-frame ATG) and other recombinant viruses shown in Fig. 5b (lanes 6 versus 5). As predicted, the elimination of the upstream in-frame ATG resulted in the elimination of the larger GP64-CAT fusion band (Fig. 5b, lane 6), confirming the origin of the larger fusion protein. These results indicate that the context of the upstream in-frame ATG, although not favorable according to Kozak's rules (40), is capable of supporting a reasonably high level of translation initiation in the late phase of the baculovirus infection. However, translation from this site appears to be leaky, since a substantial quantity of translation from the downstream site was also observed (Fig. 5b, lane 5 [upper versus lower bands]).

(ii) Cumulative CAT assay. To first examine the effects of the inactivation of both minicistron ATGs, we examined CAT activity from infected cell extracts at 24 h p.i. (Fig. 6b). We also included constructs that contained only inactivation of the minicistron initiator ATG. Each recombinant virus containing an inactivated minicistron showed increased CAT activity compared to that of the recombinant virus that contained a wild-type minicistron (Fig. 6b, vAcMC^{ATG}). Of the minicistron inactivation constructs, one virus, vAcMC$^{AaG\text{-}gTG}$, showed an increase in CAT activity of almost 3-fold, while the other viruses showed average increases of from 1.67- to 1.78-fold. This experiment demonstrated that like the single minicistron initiator mutations (vAcMC^{AaG} and vAcMC^{AgG}), the two double ATG inactivation constructs (vAcMC$^{AaG\text{-}gTG}$ and vAcMC$^{AgG\text{-}gTG}$) also resulted in increased CAT activity.

(iii) Quantitative effect of double mutations in the *gp64* minicistron. Viruses containing double mutations in the minicistron (eliminating both initiator ATG and upstream in-frame ATG) were used for quantitative analysis of translational effi-

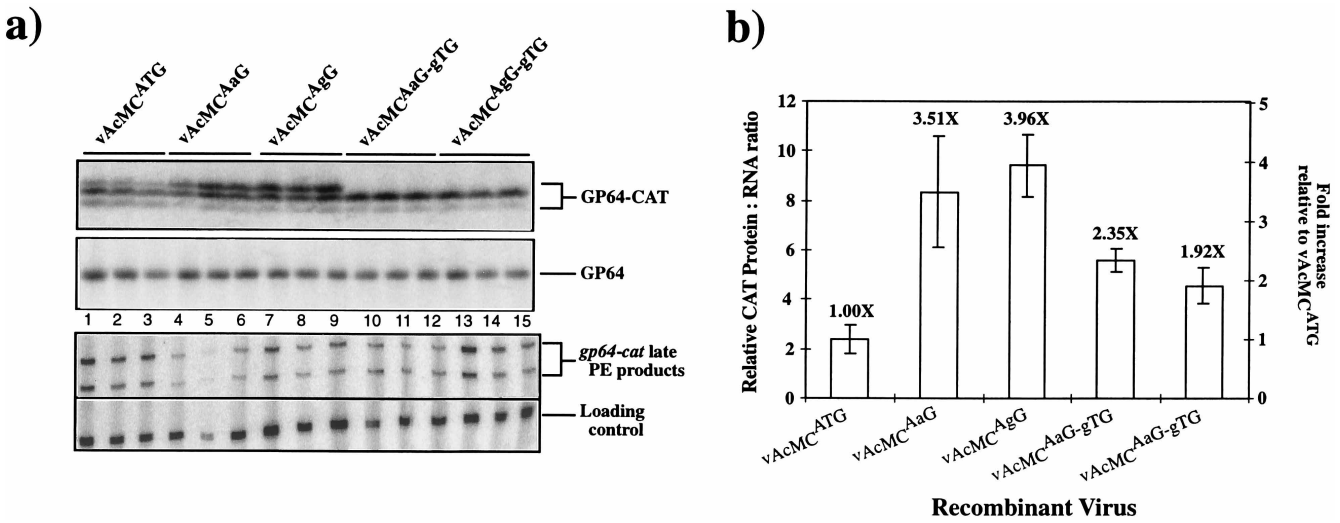

FIG. 7. Analysis of translation from viral constructs containing double minicistron mutations by quantitative immunoprecipitation. Sf9 cells were infected with recombinant viruses containing either single- or double-point mutations in the *gp64* minicistron. At 24 h p.i., total RNA was isolated and the CAT fusion proteins were immunoprecipitated. (a) Upper panel shows immunoprecipitated GP64-CAT proteins. Immunoprecipitation experiments were repeated three times for each recombinant virus. As an internal control, the GP64 protein was quantitatively immunoprecipitated from the same extracts with monoclonal antibody AcV1 (32) (middle panel). The bottom panels show primer extension (PE) products from the *gp64-cat* fusion mRNAs and the internal loading control. Translation products and RNAs from viruses containing the wild-type minicistron (vAcMC^{ATG}), single-point mutations (vAcMC^{AaG} and vAcMC^{AgG}), and double-point mutations (vAcMC$^{AaG\text{-}gTG}$ and vAcMC$^{AgG\text{-}gTG}$) are compared. (b) The CAT protein-to-RNA ratio from cells infected with each recombinant virus was compared to that from the vAcMC^{ATG} construct (designated 1.0X), and the fold increase for each recombinant virus is indicated above each bar and is indicated on the scale on the right.

ciency. Sf9 cells were infected with viruses vAcMC^{ATG}, vAcMC^{AaG}, vAcMC^{AgG}, vAcMC$^{AaG\text{-}gTG}$, and vAcMC$^{AgG\text{-}gTG}$ and pulse-labeled, and CAT proteins were immunoprecipitated (Fig. 7a, top panel). All quantitative CAT protein data were normalized to the internal GP64 protein control (Fig. 7a, middle panel). Bands representing translational initiation at the upstream in-frame ATG, the *gp64* ATG, and the CAT ATG (Fig. 5a [A, B, and C]) were quantified by PhosphorImager analysis and combined for initial calculations of translational efficiency. Corresponding quantitative primer extension analysis of the *gp64-cat* RNAs from each recombinant virus were also conducted as described above (Fig. 7a, bottom panel). A CAT protein-to-mRNA ratio was calculated for each recombinant virus as a measure of translation efficiency from the reporter mRNA. Comparisons of downstream translational efficiencies in the presence or absence of the *gp64* minicistron are shown in Fig. 7b. Inactivation of the minicistron by single-nucleotide substitutions (ATG to AaG or AgG) in the initiator codon resulted in the utilization of an upstream in-frame ATG (found within the minicistron, as described above) combined with an increase in downstream translational efficiency of approximately 3.5- to 4-fold (Fig. 7b [vAcMC^{AaG} and vAcMC^{AgG}]). Inactivation of both the minicistron initiator ATG and the upstream in-frame ATG resulted in an approximately 1.9- to 2.3-fold increase in downstream translational initiation efficiency (Fig. 7b [vAcMC$^{AaG\text{-}gTG}$ and vAcMC$^{AgG\text{-}gTG}$]). In the latter case, initiation was detected primarily at the wild-type *gp64* ATG (Fig. 7a, top panel, lanes 10 to 15).

According to the scanning model (42), ribosomes scan mRNAs 5′ to 3′ and initiate translation from the first suitable ATG encountered. In some cases, initiation at the first suitable ATG is not 100% efficient; some ribosomes may bypass the first ATG and initiate from downstream ATGs. In such cases, initiation at the upstream ATG is referred to as leaky. Because successive ATG codons were present within the leader and coding regions of *gp64-cat* late mRNAs, we used the downstream ATG initiators as trap initiator codons to measure leaky initiation from the upstream ATGs (Fig. 5a). The CAT initiator ATG (Fig. 5a [C]) is in a good Kozak context and serves as a trap to detect leaky translation initiation from the upstream *gp64* ATG initiator codon (Fig. 5a [B]). Similarly, the *gp64* ATG initiator codon can also be used as a trap initiator to measure leaky initiation from the upstream in-frame ATG (Fig. 5a [A]). Using data from quantitative immunoprecipitations (Fig. 7a) to compare the relative amounts of protein initiated at each of these sites, we calculated the relative efficiency of utilization of each ATG for each of the virus construct strategies used in this study (Fig. 8). The results from this analysis illustrate several major conclusions.

(i) Utilization of the minicistron ATG down-regulates overall translation of *gp64* and reduces or inhibits initiation from the upstream in-frame ATG. Comparison of the utilization of the upstream in-frame ATG in the wild-type construct to translation from the same site in the minicistron inactivation mutant viruses showed an approximately 8.8-fold increase in translation from the upstream in-frame site when the minicistron was inactivated (Fig. 8a, column II, UIF). Translation from the *gp64* ATG initiator also increased by 2.9-fold when the minicistron was inactivated.

(ii) Translation initiation at the minicistron ATG initiator codon was relatively efficient. Utilization of the upstream in-frame ATG initiation site was relatively low (18.8%) in the presence of the minicistron (vAcMC^{ATG} [Fig. 8a]) and increased dramatically (8.8-fold) when the minicistron ATG was inactivated (vAcMC^{ATG} [Fig. 8b]). This suggests that in the wild-type construct, the majority of the scanning ribosomes initiate at the minicistron ATG and then translate the minicistron and reinitiate downstream. Data from direct minicistron-CAT fusion experiments (Fig. 2) also support this conclusion. Initiation at the *gp64* initiator ATG is also relatively efficient. When both minicistron and upstream in-frame ATGs were eliminated (Fig. 8c), approximately 86.4% of the protein detected resulted from initiation at the *gp64* initiator ATG and only 13.6% initiated at the downstream trap ATG. In contrast,

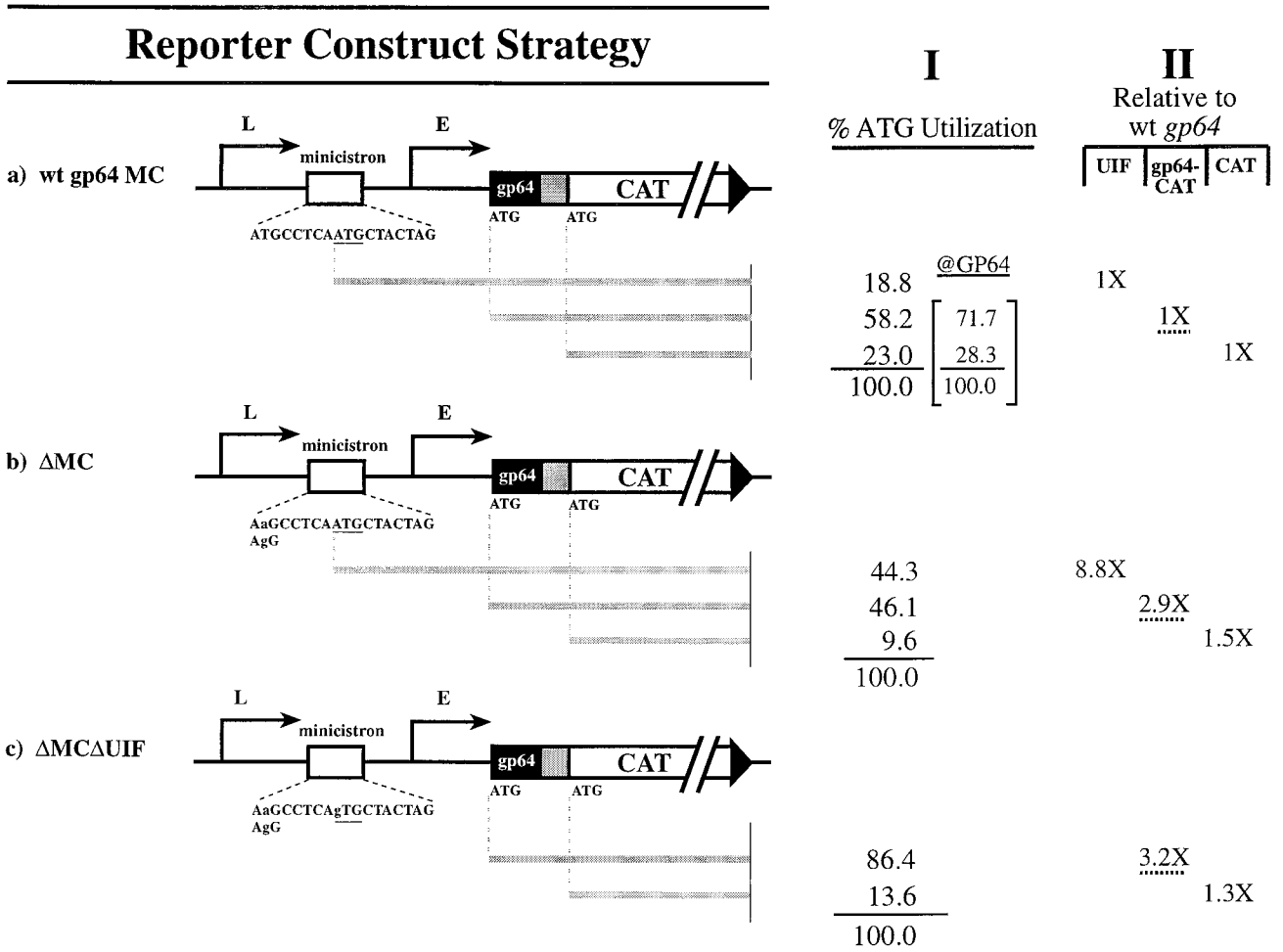

FIG. 8. Summary of translational start site utilization from *gp64* minicistron constructs containing either the wild-type minicistron (wt *gp64* MC) or single-point (ΔMC) or double-point (ΔMCΔUIF) inactivation mutations. Comparative data derived from Fig. 7a are summarized on the right for each group. Data for the wt *gp64* MC strategy are from the vAcMC^{ATG} construct. For the single mutation inactivation strategy (ΔMC), data from vAcMC^{AaG} and vAcMC^{AgG} constructs were averaged. For the double mutation inactivation strategy (ΔMCΔUIF), data from constructs vAcMC$^{AaG\text{-}gTG}$ and vAcMC$^{AgG\text{-}gTG}$ were averaged. Column I (%ATG utilization) shows the relative percentage of protein initiating at each ATG within each construct strategy. Translation from all sites within a single-construct strategy totals 100%. The total initiation downstream of the minicistron is also subdivided for the wt *gp64* MC construct. Column II shows the changes in utilization of each ATG initiator site when specific ATG initiators were inactivated. The average relative utilization of each ATG site in the wild-type construct (vAcMC^{ATG}) was assigned a value of 1×. For each construct strategy (ΔMC and ΔMCΔUIF), the fold increase in translation at each ATG position is indicated in column II.

initiation from the upstream in-frame ATG was very inefficient. When the minicistron ATG was eliminated (Fig. 8b), only approximately 44.3% of the protein detected resulted from initiation at the upstream in-frame ATG, while approximately 55.7% (46.1% plus 9.6%) initiated from downstream trap ATGs.

(iii) The relative efficiencies of translational initiation observed in this study appear to correspond generally to predictions from studies of mammalian translation initiation contexts. Of the three ATG initiation sites examined in this study, the context of the *gp64* initiator ATG (AAG**ATG**G) corresponded most closely to the general Kozak consensus (PuNN**ATG**Pu), and the initiation efficiency measured at that site was approximately 86.4% in the double mutation constructs (Fig. 8c, column I). In contrast, the context of the upstream in-frame ATG (TCA**ATG**C) did not conform to the general Kozak consensus and initiation at that site was only 44.3% efficient (Fig. 8b, column I). Although this level of initiation efficiency was poor in comparison to that from the *gp64* initiator ATG, it was unexpectedly high considering the poor context. This suggests that the stringency for translational initiation in the late phase of Ac*M*NPV infections may be significantly different from that measured in mammalian cells.

DISCUSSION

In contrast to prokaryotic RNAs, most eukaryotic mRNAs are monocistronic. Extensive experimental studies of eukaryotic mRNAs suggest that the majority of cellular mRNAs follow a scanning model for translation initiation (42, 48). In the scanning model, the protein complex known as eIF-4F binds to the m^{7}G cap structure of mRNA and mediates the assembly of a preinitiation complex that includes the 40S ribosomal subunit, tRNA^{Met}, eIF2-GTP, eIF3, and eIF1A. This complex then migrates in the 5′-to-3′ direction. When the first ATG codon in a favorable context is encountered, 60S ribosomes join the complex and translation begins. In the scanning model derived from mammalian cell systems, the optimal sequences surrounding the initiation codon are PuNNATGPu (42), and the most important positions are −3 and +4 relative to the

ATG at +1 to +3. Experimental studies in mammalian systems show that nonoptimal nucleotides in these sites usually result in failure to initiate translation (39). All evidence to date indicates that translation in baculovirus-infected insect cells supports the scanning model, since known polycistronic mRNAs do not appear to efficiently translate the downstream ORFs (23). A computer analysis of the translational initiator context of a small subset of Ac*M*NPV genes suggested that the optimal context surrounding the translation initiator ATG (AAaATGannnA) may be similar to that of vertebrate systems in which −3 and +4 positions are purine nucleotides but may include additional conserved nucleotides at positions −2 and +8 (57). However, our functional analysis of several ATG initiators that do not conform to that consensus suggest that such a consensus may not be meaningful in the absence of functional data. In the present study, we observed translational initiation from ATGs found in a poor Kozak consensus context, although that translation was leaky and led to a relatively high level of initiation at downstream trap ATG initiators. The upstream in-frame ATG within the *gp64* minicistron is found in the context 5′-TCAATGC-3′ (purine in neither the −3 nor the +4 position) yet is capable of initiating a substantial amount of translation (Fig. 7a, lanes 4 to 9, top band; Fig. 8b, ΔMC). Thus, it is unclear whether a different consensus is operable in invertebrate or baculovirus-infected cells or whether translation initiation stringency is lower or decreased during infection. We are currently examining this question. In other virus systems, leaky scanning has been shown to result in translation of more than one protein from a single ORF (12, 13, 18, 62, 63, 73). Since baculoviruses are capable of leaky scanning, it is possible that this mechanism is also used to expand the number of proteins encoded in the baculovirus genome or to regulate the levels of expression of some genes.

A small percentage of eukaryotic mRNAs contain minicistrons upstream of the major ORF. Many of these mRNAs are known proto-oncogenes which encode proteins, such as growth factors and their receptors (40). Similar mRNA structures have also been identified in eukaryotic viruses such as retroviruses (17), herpesviruses (61), hepadnaviruses (18), and reoviruses (65). The functions of most identified cellular minicistrons have not been determined; however, in some cases, translation of the upstream minicistron appears to modulate translation from the downstream ORF by down-regulating the downstream translational initiation. Experimental studies of vertebrate mRNAs containing upstream minicistrons have shown that both the minicistron and the major downstream ORFs can be translated (41, 56). The prevailing model (41) proposes that this is accomplished by translation of the upstream minicistron, followed by translational termination and partial dissociation of ribosomes and then continued ribosomal scanning and reinitiation at the downstream ORF. These studies show that a spacing of approximately 50 to 150 nt between the two ORFs is necessary for reinitiation (41, 56). Although the mechanism of reinitiation is not known, it was suggested that the 40S subunit (and certain initiation cofactors) may not dissociate from mRNA immediately after translational termination, thus permitting continued scanning and reinitiation when both the minicistron and the intracistronic distance are of an appropriate size. Thus, after translating a relatively short minicistron, scanning may continue for some distance before the ribosome dissociates completely from the mRNA. A minimum spacing of 50 to 80 nt may enable the 40S subunit to acquire $tRNA^{Met}$ after translating the upstream minicistron, whereas a spacing of more than 150 nt may allow the 40S subunit to dissociate from the mRNA (41). Longer or shorter spacing between cistrons usually inhibits reinitiation and translation of the downstream ORF. In the Ac*M*NPV *gp64* gene, the minicistron is located 44 nt upstream of the *gp64* ORF. Thus, if translation of the Ac*M*NPV *gp64* gene conforms to the minicistron model proposed for mammalian mRNAs (41), the intracistronic distance is relatively short and this should negatively affect reinitiation. Because we did not alter intracistronic spacing in this study, it is not yet possible to determine whether such spacing plays a role in the demonstrated lower initiation efficiency at the downstream *gp64* initiator ATG when the minicistron is present. It is also possible that optimal intracistronic spacing may differ in invertebrate cells or in baculovirus-infected insect cells. The spacing required for ribosomal subunits to become competent for reinitiation may also vary, depending on the secondary structure of a specific mRNA. In the *gp64* gene from the related virus, Op*M*NPV, the intracistronic spacing is slightly longer than that in Ac*M*NPV (67 versus 44 nt, respectively).

Some of the most intensively studied minicistrons are those from the yeast *GCN4* gene, Rous sarcoma virus (RSV), and human cytomegalovirus (CMV). In each case, several minicistrons are found in the 5′ leader region of important mRNAs. The yeast gene *GCN4* contains four upstream minicistrons, and the first and the fourth minicistrons regulate the translation of *GCN4* based on the availability of nutrients (31). In viral systems, minicistrons may have a number of different functions. In RSV, three small minicistrons are located upstream of the *gag* gene (17). Two of the three minicistrons appear to serve a role as enhancers of translational initiation from the *gag* gene, since their inactivation results in decreased *gag* production and decreased RNA packaging. Thus, these retrovirus minicistrons may play a role in the regulation of virion production. In the human CMV, several genes contain minicistrons in their 5′ leader regions. Three minicistrons are found in the leader of the *gp48* gene. The second minicistron is conserved among CMV strains and was shown to play a negative regulatory role in translation of the *gp48* (10, 11, 61).

A number of RNAs encoded by Ac*M*NPV genes contain minicistrons (Table 1), suggesting that minicistrons play a role in the translational regulation of these genes. Because the *gp64* promoter-minicistron structure is conserved among all baculoviruses that have been examined, we hypothesized that the minicistron would play a role in translational regulation from *gp64* late mRNAs. In the current study, we used a recombinant virus containing a minicistron-CAT fusion to demonstrate that the minicistron from the Ac*M*NPV *gp64* gene is in a context suitable for efficient translation and that the minicistron is likely translated during the late phase. By inserting discrete substitution mutations that inactivated the minicistron initiator ATG and generating the appropriate recombinant viruses, we showed that minicistron inactivation resulted in increased translational efficiency from downstream ATGs. Thus, the data presented here indicate that the Ac*M*NPV *gp64* minicistron negatively regulates translation of the *gp64* ORF. This negative effect may result from either a delay in translation caused by the requirement for initiation and translation of the minicistron or by inefficient reinitiation at the downstream ORF. Such inefficient reinitiation could result from a suboptimal intracistronic spacing between the minicistron and *gp64* ORF. However, analysis of the percentage of ATG utilization at the wild-type *gp64* ATG and the downstream CAT trap ATG (the wild-type CAT initiator ATG) suggests that the efficiency of initiation at the *gp64* ATG is not substantially different in the presence or absence of the minicistron (71.7 versus 86.4% [Fig. 8a versus c]). If intracistronic spacing plays a substantial role in translational reinitiation efficiency, we might expect to see a much higher level of utilization of the downstream CAT trap

ATG when the minicistron was present, since the spacing between the minicistron and the trap ATG is greater (80 nt). Although utilization of the CAT trap ATG is higher in the wild-type construct, the difference is not large. Thus, while we cannot discount this difference, it appears that the overall negative effect of the minicistron on downstream translational initiation may result from a delay in the travel of the ribosome, since it initiates and translates the minicistron. It is also possible that the peptide encoded by the minicistron plays a role in this negative effect. Indeed, in the human CMV *gp48* gene, the yeast *CPA-1* gene, and the human *S*-adenosylmethionine decarboxylase gene, negative regulation of downstream ORFs is closely related to the peptides encoded by minicistrons (15, 16, 30, 69). In the present study, we did not examine the effect of the coding sequence. Although the minicistron coding sequence is not conserved in *gp64* genes from all baculoviruses examined, we cannot exclude the possibility that these small three- to five-amino-acid peptides play a role in negative regulation by the minicistron.

The observation that the *gp64* minicistron negatively regulates translation from the downstream *gp64* ORF during the late phase is surprising. It is not clear why *gp64* translation should be negatively regulated during the late phase, when budded virions are produced. A possible explanation is that overproduction or inappropriate temporal production of GP64 may interfere either with virion budding or with the production of the occluded form of the virus during the very late phase of the infection cycle. Alternatively, this translational regulation may modulate entry of GP64 into the secretory pathway. The conservation of the minicistron structure on late *gp64* mRNAs of different baculoviruses suggests that the presence of this regulatory element provides a selective advantage.

ACKNOWLEDGMENTS

We thank David Garrity and Casey Finnerty for comments on the manuscript and George Rohrmann for providing the Op*M*NPV genomic sequence prior to release.

This research was supported by grants from NIH (AI31130) and USDA (9601885).

REFERENCES

1. **Ahrens, C. H., R. L. Q. Russell, C. J. Funk, J. T. Evans, S. H. Harwood, and G. F. Rohrmann.** 1997. The sequence of the *Orgyia pseudotsugata* multinucleocapsid nuclear polyhedrosis virus genome. Virology **229:**381–399.
2. **Aquilla, T. T.** 1989. Molecular cloning of the 64-kilodalton envelope glycoprotein of *Rachiplusia ou* nuclear polyhedrosis virus. M.A. thesis. University of California, Riverside, Calif.
3. **Arrick, B. A., A. L. Lee, R. L. Grendell, and R. Derynck.** 1991. Inhibition of translation of transforming growth factor-β3 mRNA by its 5′ untranslated region. Mol. Cell. Biol. **11:**4306–4313.
4. **Ayres, M. D., S. C. Howard, J. Kuzio, M. Lopez-Ferber, and R. D. Possee.** 1994. The complete DNA sequence of *Autographa californica* nuclear polyhedrosis virus. Virology **202:**586–605.
5. **Beniya, H., C. J. Funk, G. F. Rohrmann, and R. F. Weaver.** 1996. Purification of a virus-induced RNA polymerase from *Autographa californica* nuclear polyhedrosis virus-infected *Spodoptera frugiperda* cells that accurately initiates late and very late transcription *in vitro*. Virology **216:**12–19.
6. **Blissard, G. W., P. H. Kogan, R. Wei, and G. F. Rohrmann.** 1992. A synthetic early promoter from a baculovirus: roles of the TATA box and conserved start site CAGT sequence in basal levels of transcription. Virology **190:**783–793.
7. **Blissard, G. W., R. L. Quant-Russell, G. F. Rohrmann, and G. S. Beaudreau.** 1989. Nucleotide sequence, transcriptional mapping, and temporal expression of the gene encoding P39, a major structural protein of the multicapsid nuclear polyhedrosis virus of *Orgyia pseudotsugata*. Virology **168:**354–362.
8. **Blissard, G. W., and G. F. Rohrmann.** 1989. Location, sequence, transcriptional mapping, and temporal expression of the *gp64* envelope glycoprotein gene of the *Orgyia pseudotsugata* multicapsid nuclear polyhedrosis virus. Virology **170:**537–555.
9. **Blissard, G. W., and G. F. Rohrmann.** 1991. Baculovirus *gp64* gene expression: analysis of sequences modulating early transcription and transactivation by IE1. J. Virol. **65:**5820–5827.
10. **Cao, J., and A. P. Geballe.** 1994. Mutational analysis of the translational signal in the human cytomegalovirus gpUL4 (gp48) transcript leader by retroviral infection. Virology **205:**151–160.
11. **Cao, J., and A. P. Geballe.** 1996. Coding sequence-dependent ribosomal arrest at termination of translation. Mol. Cell. Biol. **16:**603–608.
12. **Carroll, R., and D. Derse.** 1993. Translation of equine infectious anemia virus bicistronic Tat-Rev mRNA requires leaky ribosome scanning of the Tat CTG initiation codon. J. Virol **67:**1433–1440.
13. **Chenik, M., K. Chebi, and D. Blondel.** 1995. Translation initiation at alternate in-frame AUG codons in the rabies virus phosphoprotein mRNA is mediated by a ribosomal leaky scanning mechanism. J. Virol. **69:**707–712.
14. **Chisholm, G. E., and D. J. Henner.** 1988. Multiple early transcripts and splicing of the *Autographa californica* nuclear polyhedrosis virus IE-1 gene. J. Virol. **62:**3193–3200.
15. **Degnin, C. R., M. R. Schleiss, J. Cao, and A. P. Geballe.** 1993. Translational inhibition mediated by a short upstream open reading frame in the human cytomegalovirus GpUL4 gp48 transcript. J. Virol. **67:**5514–5521.
16. **Delbecq, P., M. Werner, A. Feller, R. K. Filipkowski, F. Messenguy, and A. Pierard.** 1994. A segment of mRNA encoding the leader peptide of the CPA1 gene confers repression by arginine on a heterologous yeast gene transcript. Mol. Cell. Biol. **14:**2378–2390.
17. **Donze, O., and P. F. Spahr.** 1992. Role of the open reading frames of Rous sarcoma virus leader RNA in translation and genome packaging. EMBO J. **11:**3747–3757.
18. **Fouillot, N., S. Tlouzeau, J. M. Rossignol, and J. O. Jean.** 1993. Translation of the hepatitis B virus *p* gene by ribosomal scanning as an alternative to internal initiation. J. Virol. **67:**4886–4895.
19. **Friesen, P. D., and L. K. Miller.** 1985. Temporal regulation of baculovirus RNA: overlapping early and late transcripts. J. Virol. **54:**392–400.
20. **Fuchs, L. Y., M. S. Woods, and R. F. Weaver.** 1983. Viral transcription during *Autographa californica* nuclear polyhedrosis virus infection: a novel RNA polymerase induced in infected *Spodoptera frugiperda* cells. J. Virol. **48:**641–646.
21. **Garrity, D. B., M.-J. Chang, and G. W. Blissard.** 1997. Late promoter selection in the baculovirus *gp64* envelope fusion protein gene. Virology **231:**167–181.
22. **Gombart, A. F., G. W. Blissard, and G. F. Rohrmann.** 1989. Characterization of the genetic organization of the Hind-III M region of the multicapsid nuclear polyhedrosis virus of *Orgyia pseudotsugata* reveals major differences among baculoviruses. J. Gen. Virol. **70:**1815–1828.
23. **Gross, C., and G. F. Rohrmann.** 1993. Analysis of the role of 5′ promoter elements and 3′ flanking sequences on the expression of a baculovirus polyhedrin envelope protein gene. Virology **192:**273–281.
24. **Grula, M. A., P. L. Buller, and R. F. Weaver.** 1981. Alpha amanitin-resistant viral RNA synthesis in nuclei isolated from nuclear polyhedrosis virus-infected *Heliothis zea* larvae and *Spodoptera frugiperda* cells. J. Virol. **38:**916–921.
25. **Guarino, L. A., and M. W. Smith.** 1990. Nucleotide sequence and characterization of the *39k* gene region of *Autographa californica* nuclear polyhedrosis virus. Virology **179:**1–8.
26. **Guarino, L. A., and M. D. Summers.** 1986. Functional mapping of a trans-activating gene required for expression of a baculovirus delayed-early gene. J. Virol. **57:**563–571.
27. **Guzo, D., H. Rathburn, K. Guthrie, and E. Dougherty.** 1992. Viral and host cellular transcription in *Autographa californica* nuclear polyhedrosis virus-infected gypsy moth cell lines. J. Virol. **66:**2966–2972.
28. **Harigai, M., T. Miyashita, M. Hanada, and J. C. Reed.** 1996. A cis-acting element in the Bcl-2 gene controls expression through translational mechanisms. Oncogene **12:**1369–1374.
29. **Hill, J. E., and P. Faulkner.** 1994. Identification of the *gp67* gene of a baculovirus pathogenic to the spruce budworm, *Choristoneura fumiferana* multinucleocapsid nuclear polyhedrosis virus. J. Gen. Virol. **75:**1811–1813.
30. **Hill, J. R., and D. R. Morris.** 1993. Cell-specific translational regulation of adenosylmethionine decarboxylase mRNA dependence on translation and coding capacity of the cis-acting upstream open reading frame. J. Biol. Chem. **268:**726–731.
31. **Hinnebusch, A. G.** 1996. Translational control of GCN4: gene-specific regulation by phosphorylation of eIF2. Cold Spring Harbor Monogr. Ser. **30:** 199–244.
32. **Hohmann, A. W., and P. Faulkner.** 1983. Monoclonal antibodies to baculovirus structural proteins: determination of specificities by Western blot analysis. Virology **125:**432–444.
33. **Huh, N. E., and R. F. Weaver.** 1990. Identifying the RNA polymerases that synthesize specific transcripts of the *Autographa californica* nuclear polyhedrosis virus. J. Gen. Virol. **71:**195–202.
34. **Jarvis, D. L., and A. Garcia.** 1994. Biosynthesis and processing of the *Autographa californica* nuclear polyhedrosis virus GP64 protein. Virology **205:** 300–313.
35. **Kamita, S. G., and S. Maeda.** 1993. Inhibition of *Bombyx mori* nuclear polyhedrosis virus (NPV) replication by the putative DNA helicase gene of *Autographa californica* NPV. J. Virol. **67:**6239–6245.
36. **Kitts, P. A., and R. D. Possee.** 1993. A method for producing recombinant

baculovirus expression vectors at high frequency. BioTechniques **14:**810–817.
37. **Kogan, P. H., and G. W. Blissard.** 1994. A baculovirus *gp64* early promoter is activated by host transcription factor binding to CACGTG and GATA elements. J. Virol. **68:**813–822.
38. **Kogan, P. H., X. Chen, and G. W. Blissard.** 1995. Overlapping TATA-dependent and TATA-independent early promoter activities in the baculovirus *gp64* envelope fusion protein gene. J. Virol. **69:**1452–1461.
39. **Kozak, M.** 1986. Point mutations define a sequence flanking the AUG initiator codon that modulates translation by eukaryotic ribosomes. Cell **44:**283–292.
40. **Kozak, M.** 1987. An analysis of 5′-noncoding sequences from 699 vertebrate messenger RNAs. Nucleic Acids Res. **15:**8125–8132.
41. **Kozak, M.** 1987. Effects of intercistronic length on the efficiency of reinitiation by eukaryotic ribosomes. Mol. Cell. Biol. **7:**3438–3445.
42. **Kozak, M.** 1989. The scanning model for translation: an update. J. Cell Biol. **108:**229–241.
43. **Li, Y., and L. K. Miller.** 1995. Expression and functional analysis of a baculovirus gene encoding a truncated protein kinase homolog. Virology **206:**314–323.
44. **Lu, A., and E. B. Carstens.** 1992. Transcription analysis of the *Eco*RI D region of the baculovirus *Autographa californica* nuclear polyhedrosis virus identifies an early 4-kilobase RNA encoding the essential *p143* gene. J. Virol. **66:**655–663.
45. **Lu, A., and L. K. Miller.** 1995. The roles of eighteen baculovirus late expression factor genes in transcription and DNA replication. J. Virol. **69:**975–982.
46. **Majima, K., S. Gomi, T. Ohkawa, S. G. Kamita, and S. Maeda.** 1996. Complete nucleotide sequence of the 128,413 bp-long genome of the baculovirus BmNPV. Genbank accession no. L33180.
47. **Marth, J. D., R. W. Overell, K. E. Meier, E. G. Krebs, and R. M. Perlmutter.** 1988. Translational activation of the *lck* proto-oncogene. Nature **332:**171–173.
48. **Merrick, W. C., and J. W. B. Hershey.** 1996. The pathway and mechanism of eukaryotic protein synthesis. Cold Spring Harbor Monogr. Ser. **30:**31–69.
49. **Miller, L. K.** 1996. Insect viruses, p. 533–556. *In* B. N. Fields, D. M. Knipe, and P. M. Howley (ed.), Virology, 3rd ed. Lippincott-Raven, New York, N.Y.
50. **Monsma, S. A., and G. W. Blissard.** 1995. Identification of a membrane fusion domain and an oligomerization domain in the baculovirus GP64 envelope fusion protein. J. Virol. **69:**2583–2595.
51. **Morris, T. D., and L. K. Miller.** 1994. Mutational analysis of a baculovirus major late promoter. Gene **140:**147–153.
52. **Neumann, J. R., C. A. Morency, and K. O. Russian.** 1987. A novel rapid assay for chloramphenicol acetyltransferase gene expression. BioTechniques **5:** 444–447.
53. **Oellig, C., B. Happ, T. Mueller, and W. Doerfler.** 1987. Overlapping sets of viral RNAs reflect an array of polypeptides in the *Eco*RI J and N fragments (map positions 81.2 to 85.0) of the *Autographa californica* nuclear polyhedrosis virus genome. J. Virol. **61:**3048–3057.
53a. **Oomens, A. G. P.** Personal communication.
54. **Oomens, A. G. P., S. A. Monsma, and G. W. Blissard.** 1995. The baculovirus GP64 envelope fusion protein: synthesis, oligomerization, and processing. Virology **209:**592–603.
55. **O'Reilly, D. R., L. K. Miller, and V. A. Luckow.** 1992. Baculovirus expression vectors, a laboratory manual. W. H. Freeman & Co., New York, N.Y.
56. **Peabody, D. S., S. Subramani, and P. Berg.** 1986. Effect of upstream reading frames on translation efficiency in simian virus 40 recombinants. Mol. Cell. Biol. **6:**2704–2711.
57. **Ranjan, A., and S. E. Hasnain.** 1994. Influence of codon usage and translation initiation codon context in the *Ac*NPV-based expression system: computer analysis using homologous and heterologous genes. Virus Genes **9:** 149–153.
58. **Rankin, C., B. G. Ooi, and L. K. Miller.** 1988. Eight base pairs encompassing the transcriptional start point are the major determinant for baculovirus polyhedrin gene expression. Gene **70:**39–49.
59. **Ray, F. A., and J. A. Nickoloff.** 1992. Site-specific mutagenesis of almost any plasmid using a PCR-based version of unique site elimination. BioTechniques **13:**342–346.
60. **Rohrmann, G. F.** 1986. Polyhedrin structure. J. Gen. Virol. **67:**1499–1513.
61. **Schleiss, M. R., C. R. Degnin, and A. P. Geballe.** 1991. Translational control of human cytomegalovirus gp48 expression. J. Virol. **65:**6782–6789.
62. **Schwartz, S., B. K. Felber, and G. N. Pavlakis.** 1992. Mechanism of translation of monocistronic and multicistronic human immunodeficiency virus type 1 mRNAs. Mol. Cell. Biol. **12:**207–219.
63. **Sedman, S. A., P. J. Good, and J. E. Mertz.** 1989. Leader-encoded open reading frames modulate both the absolute and relative rates of synthesis of the virion proteins of simian virus 40. J. Virol. **63:**3884–3893.
64. **Sivasubramanian, N.** 1988. Organization of the envelope protein gene (*gp64*) in the *Autographa californica* MNPV, p. 103. *In* Abstracts of the 21st Annual Meeting of the Society for Invertebrate Pathology.
65. **Suzuki, N., M. Tanimura, Y. Watanabe, T. Kusano, Y. Kitagawa, N. Suda, H. Kudo, I. Uyeda, and E. Shikata.** 1992. Molecular analysis of rice dwarf phytoreovirus segment S1 interviral homology of the putative RNA-dependent RNA polymerase between plant and animal-infecting reoviruses. Virology **190:**240–247.
66. **Thiem, S. M., and L. K. Miller.** 1989. Identification, sequence, and transcriptional mapping of the major capsid protein gene of the baculovirus *Autographa californica* nuclear polyhedrosis virus. J. Virol. **63:**2008–2018.
67. **Todd, J. W., A. L. Passarelli, and L. K. Miller.** 1995. Eighteen baculovirus genes, including lef-11, p35, 39K, and p47, support late gene expression. J. Virol. **69:**968–974.
68. **Weaver, R. F., and C. Q. Jun.** 1982. Capping of viral RNA in cultured *Spodoptera frugiperda* cells infected with *Autographa californica* nuclear polyhedrosis virus. J. Virol. **43:**234–240.
69. **Werner, M., A. Feller, F. Messenguy, and A. Pierard.** 1987. The leader peptide of yeast gene CPA-1 is essential for the translational repression of its expression. Cell **49:**805–814.
70. **Whitford, M., S. Stewart, J. Kuzio, and P. Faulkner.** 1989. Identification and sequence analysis of a gene encoding *gp67*, an abundant envelope glycoprotein of the baculovirus *Autographa californica* nuclear polyhedrosis virus. J. Virol. **63:**1393–1399.
71. **Wu, J., and L. K. Miller.** 1989. Sequence, transcription, and translation of a late gene of the *Autographa californica* nuclear polyhedrosis virus encoding a 34.8k polypeptide. J. Gen. Virol. **70:**2449–2460.
72. **Yang, C. L., D. A. Stetler, and R. F. Weaver.** 1991. Structural comparison of the *Autographa californica* nuclear polyhedrosis virus-induced RNA polymerase and the three nuclear RNA polymerases from the host *Spodoptera frugiperda*. Virus Res. **20:**251–264.
73. **Zhou, H., and A. L. Jackson.** 1996. Expression of the barley stripe mosaic virus RNA-beta "triple gene block." Virology **216:**367–379.
74. **Zuidema, D., A. Schouten, M. Usmany, A. J. Maule, G. J. Belsham, J. Roosien, E. C. Klinge Roode, J. W. M. Van Lent, and J. M. Vlak.** 1990. Expression of cauliflower mosaic virus gene I in insect cells using a novel polyhedrin-based baculovirus expression vector. J. Gen. Virol. **71:**2201–2210.